Interfacial thermal transport and structural preferences in carbon nanotube—polyamide-6,6 nanocomposites: How important are chemical functionalization effects?

4 **AUTHORS**, INCLUDING:

Mohammad Alaghemandi

University of Massachusetts Boston

18 PUBLICATIONS   **237** CITATIONS

Interfacial thermal transport and structural preferences in carbon nanotube–polyamide-6,6 nanocomposites: how important are chemical functionalization effects?

Mohammad Reza Gharib-Zahedi,[a] Mohsen Tafazzoli,*[a] Michael C. Böhm[b] and Mohammad Alaghemandi[c]

We employ reverse nonequilibrium molecular dynamics simulations to investigate the interfacial heat transfer in composites formed by an ungrafted or a grafted carbon nanotube which is surrounded by oligomeric polyamide-6,6 chains. The structural properties of the polymer matrix and the grafted chains are also studied. The influence of the grafting density, the length of the grafted chains as well as their chemical composition on the interfacial thermal conductivity (λ_i) are in the focus of our computational study. For the considered grafted polyethylene and polyamide chains we do not find a sizeable difference in the observed λ_i values. In contrast to this insensitivity, we predict a rather strong influence on λ_i by the grafting density and the length of the grafted chains. This dependence is an outcome of modifications in the structural properties of the polymer matrix as well as the grafted chains. Functionalization of the nanotube has a sizeable influence on the interfacial thermal conductivity. Its enhancement is caused by the chemical bonds between the nanotube and grafted chain atoms which reduce the number of Kapitza resistances hindering the heat transfer in polymer samples. The phonon density of states profiles confined to the bonded nanotube and the grafted chain atoms are used to emphasize the phonon support of the thermal conductivity in nanocomposites with grafted tubes. Strategies to tailor nanotube containing composites with higher thermal conductivities than that realized in the bare polymer are shortly touched.

1. Introduction

Nanocomposites have attracted increasing scientific and technological attention for a variety of applications as novel devices and performance materials with properties that can be tailored. The addition of carbon nanotubes (CNTs) to a polymer matrix generates not only new functionalities but also an improvement in the mechanical,[1–5] electrical,[6–8] and thermal[9–13] behavior of the host polymer. In a number of experimental and theoretical studies it has been emphasized that the particularly high thermal conductivity (λ) of an isolated CNT is caused by an efficient phonon support *via* delocalized modes.[14,15] In contrast to the exceptional heat transfer in CNT or graphene samples,[16,17] polymers such as polyethylene (PE) or polyamide-6,6 (PA) have

rather low thermal conductivities.[18,19] Their λ values do not exceed 0.4 to 0.5 W m^{-1} K^{-1}.[18] This strong attenuation is an implication of the large thermal (Kapitza) resistance between neighboring polymer chains only coupled by weak van der Waals interactions. Mode delocalization over neighboring chains is not possible under these circumstances. In such materials the thermal conductivity is supported by interchain collisions which, however, are hindered in their efficiency by interchain Kapitza resistances. With an increasing number of such resistances, λ is more and more reduced.

A moderate λ enhancement in polymers due to phonon modes has been detected in certain anisotropic materials.[19–22] An anisotropy in the thermal conductivity has been found in stretched polystyrene (PS) materials in the framework of reverse nonequilibrium molecular dynamics (RNEMD) simulations.[23] The preferential orientation of PS chains in the stretching direction leads to an increase in the number of chemical bonds. At the same time, the number of the nonbonded interchain contacts in the perpendicular planes is enhanced.[19] Under these spatial conditions a larger number of "delocalized" modes than in the isotropic parent is formed in the stretching direction while more

[a] *Department of Chemistry, Sharif University of Technology, 11365-9516 Tehran, Iran. E-mail: tafazzoli@sharif.edu*

[b] *Eduard-Zintl-Institut für Anorganische und Physikalische Chemie, Technische Universität Darmstadt, D-64287 Darmstadt, Germany*

[c] *Department of Chemistry, University of Massachusetts Boston, Boston, Massachusetts 02125, USA*

Kapitza resistances occur perpendicular to the stretching. As a matter of fact, the thermal conductivity in the stretching direction is higher than λ in the isotropic polymer phase. In contrast to this enhancement the thermal conductivity in the perpendicular direction is reduced.[19]

Despite these well-known physical principles controlling the thermal conductivity in polymers, CNT composites have been synthesized with the intention to observe λ values significantly larger than λ of the host polymer.[10–13] Even in the absence of chemical bonds between the different polymer components the phonon density of states (DOS) profiles have been employed to explain or to predict the heat transfer in these systems.[10,24,25] The non-validity of such a brute force argumentation has recently been demonstrated for CNT–polymer composites where the interfacial thermal conductivity between neighboring CNT chains is small as a result of the influence of the surrounding matrix.[26] Identical phonon DOS profiles of adjacent CNT chains cannot be used as a criterion to expect exceptionally high λ values.[26,27] When considering the information mentioned above, it should not be a surprise that neither experiments nor computer studies of the MD type on CNT–polymer composites reported λ values significantly larger than in the bare polymer. Even one of the largest λ enhancements of 100% relative to the bare polymer matrix is much smaller than expected on the basis of interpolation schemes employing the component mass or volume ratios.[28,29] The same general trends were observed in experimental studies of other systems.[30–32]

Despite these discouraging observations let us summarize some properties supporting an enhancement of λ in the neighborhood of CNTs. The tube alone occupies a spatial region without Kapitza resistances, *i.e.*, we have a region allowing mode delocalization.[33] Transversal nanotube modes at low wave numbers can act as a minor enhancement factor for the interfacial heat transport.[14] Furthermore, the CNT chains force an enhanced polymer ordering in their vicinity.[26] Often the polymers prefer a tangential or perpendicular orientation relative to the CNT chains. Irrespective of the sign of the CNT–polymer interaction, the mass density of the matrix near the tube is larger than the bulk density. Similar to the stretched PS sample just mentioned,[19] a stronger increase of λ in the polymer is hindered due to the influence of Kapitza resistances. Nevertheless, one should take into account that the three factors just summarized (*i.e.*, presence of CNTs allowing the formation of delocalized modes, polymer mass enhancement and ordering in the interphase) generate a local interfacial thermal conductivity exceeding slightly the isotropic λ value of the bare polymer. In the longitudinal CNT direction the observed λ values are smaller than in an isolated tube.[26]

In order to enhance the interfacial thermal conductivity in CNT–polymer composites, it is necessary to strengthen the interaction between the bare tube and the surrounding matrix. This can be done by CNT grafting with polymer chains. In such a sample the CNT molecule is coupled by chemical bonds to some of the polymer chains allowing a more efficient mode coupling with polymer chains in its neighborhood. The number of λ reducing Kapitza resistances is thereby reduced. The necessary

CNT pyramidalization furthermore increases the reactivity of the tube.[34] It can become more reactive than a graphene sheet. The covalent functionalization of CNTs provides a way to engineer the CNT–polymer interface for favorable mechanical[35–38] and thermal[39–41] composite properties. The tensile strength of a polyethylene matrix with incorporation of 10 weight (wt)% carboxylated multi-walled CNTs, *e.g.*, is enhanced by 108%.[35] Gao *et al.*[36] added 1 wt% carboxylated CNT to a PA matrix to observe an increase in the Young's modulus of 153% and a 103% increase in the tensile strength. The reduction of the interfacial resistance between functionalized CNTs and a polymer matrix has been found in other recent experimental studies.[42,43] Huang *et al.*[41] discussed such an enhanced coupling between CNT chains grafted by poly(ethyleneimine) and an epoxy matrix, *i.e.*, conditions favouring an enhanced thermal conductivity.

Theoretical investigations in line with experimental efforts have been performed to study the characteristics of the heat transport at the interface between functionalized CNTs or graphenes and the surrounding polymer.[25,44–51] Results from analytical models based on an effective medium theory,[44,51] a micromechanical modeling approach[45,46] as well as atomistic simulations[25,47–51] have emphasized that functionalized CNTs in a polymer matrix modify the thermal properties of the interfacial polymer phase relative to λ of its bare parent system. MD simulations and an effective medium theory predicted an increase in the thermal conductivity by roughly a factor of two in a composite containing a functionalized single-walled CNT.[44,48] In a micromechanical approach, Seidel and Lagoudas[45] have shown that the functionalization of the CNT surface (*i.e.*, the interface coupling between the reinforcing component and the matrix, as well as the CNT hollowness, see above) has significant effects on the thermal conductivity of the composite. Recently – in combination with other investigators – Khare *et al.*[48] have shown a similar behavior. Luo and Lloyd[49] investigated the thermal properties of graphene/graphite–paraffin systems by MD simulations. Their results provided evidence that an improved interfacial conductivity is accessible by chemical bonds in the interface, by polymer density enhancement as well as by graphene elongation. Furthermore, for functionalized graphene–polymer composites, Wang *et al.*[50] considered different grafting densities of linear hydrocarbon chains in their analysis of composites containing monolayer graphene. They found a critical value in the filler length; if exceeded, the influence of the graphene functionalization as an enhancement factor of λ becomes inefficient. The influence of the grafted chain length on the interfacial thermal transport in graphene–polymer nanocomposites has been studied in a very recent work of Wang *et al.*[51] Possibilities to enhance the interfacial thermal conductivity by CNT surfaces that have different chemical compositions of the grafted chains as well as different grafted chain lengths and grafting densities, however, have not been considered until now. Notably, structural modifications of polymer chains in the CNT–polyamide interphase and their influence on λ are an essential part of the present article.

Thus we investigate the influence of chemically functionalized CNTs on the structural properties of the surrounding PA matrix as well as the interfacial thermal conductivity of PA–CNT

composites. The powerful RNEMD formalism[23] is adopted to derive the λ values. The study at hand is an extension of our recent work on CNTs[14,27,52] and CNT–PA nanocomposites.[26] Systematic atomistic MD calculations have been performed to improve our understanding of the structural and thermal properties of a PA matrix surrounding either an ungrafted (bare) or a grafted CNT. Different grafting densities as well as two types of grafted chains, *i.e.*, PA and PE, have been chosen for our computer simulations. Amide linker units have been adopted to bind PA or PE to the nanotube. The CNTs are either ungrafted or they are grafted by PA or PE chains of similar lengths, which, however, differ from the length of the PA matrix chains. All simulations have been carried out at a temperature of 350 K and a pressure of 101.3 kPa. We have employed the YASP molecular dynamics code.[53] The chosen simulation conditions allowed us to compare the present results with previous findings.[26] Different structural properties have been analyzed with the aim to rationalize variations in the thermal transport properties under the influence of functionalized nanotubes. In contrast to highly questionable phonon density of states arguments in systems where neighboring chains interact only by van der Waals contacts, the chemical bonds between the CNT and the grafted polymer chains allowed us a qualitative interpretation of the thermal conductivity data on the basis of phonon DOS profiles. In such composite systems degeneracies between CNT modes and modes of the surrounding grafted polymer chains can be used to explain the λ profile of the PA matrix.

The organization of the present article is as follows. The theoretical background of our simulations is explained in the next section. Computational conditions are summarized in Section 3. Section 4 providing the results and discussion is divided into three subsections. In Section 4.1 we discuss the polymer density around the nanotube. Structural details of the polymer matrix as well as of the grafted chains are the topic of Section 4.2 while the interfacial thermal conductivity in the studied nanocomposites is analyzed in the last Section 4.3. The article ends with a short summary and conclusions.

2. Theoretical background

We have used the reverse nonequilibrium molecular dynamics method to derive the interfacial thermal conductivity λ_i of the chosen nanocomposite systems in which a PA polymer matrix is in contact with either a bare (ungrafted) or a PE (PA) grafted CNT. A precise definition of λ_i will be given somewhat later. The RNEMD approach makes use of a reversal of the experimental cause-and-effect principle. It imposes an artificial heat flow between different regions (slabs) of the simulation box as a primary perturbation. The RNEMD algorithm requires an exchange of the velocities of the coldest particle (smallest kinetic energy) from the chosen hot slab and the hottest particle (largest kinetic energy) from the cold area. As there is only a velocity exchange between particles (N) of the same mass, the total energy (E) is conserved. In the steady state, the same

amount of the energy per unit time and cross-sectional area as exchanged under *NE* conditions is transferred *via* heat conduction from the hot to the cold region. From the known heat flow j_z with z denoting the direction of the heat transport and the temperature gradient $(\mathrm{d}T/\mathrm{d}z)$ the thermal conductivity λ_z can be calculated.

$$j_z = \frac{1}{2tA} \sum_{\text{transfer}} \frac{m}{2} \left(v_{\text{hot}}^2 - v_{\text{cold}}^2 \right), \qquad (1)$$

$$\lambda_z = -\frac{j_z}{\left\langle \dfrac{\mathrm{d}T}{\mathrm{d}z} \right\rangle}, \qquad (2)$$

In eqn (1) m labels the mass of the exchanged particles, t the simulation time and A the cross-sectional area perpendicular to the heat flux. The velocities of the hot and cold particles are symbolized by v_{hot} and v_{cold}. In the most general case the summation in eqn (1) is over all transfer processes. To derive the interfacial heat transfer in the present work, eqn (2) has to be modified; see below. Detailed information, how to calculate λ_i, can be found in our recent work.[26] We have adopted $\langle \ldots \rangle$ to denote thermal averaging.

To evaluate the heat transfer at CNT–polymer interfaces, we have defined λ_i as

$$\lambda_i = -\frac{j}{\left\langle \dfrac{\Delta T}{\Delta R} \right\rangle}, \qquad (3)$$

The quantity λ_i is defined by the ratio between the energy flux through a cylindrical surface and the temperature gradient between the CNT and the first surrounding PA layer ΔR. In the studied composites ΔR is identified as the distance between the CNT surface and the first density peak in the radial distribution function (RDF). As a matter of fact, ΔT and ΔR measure the temperature difference and distance between two chosen interfacial layers (*i.e.*, the CNT atoms and the first polymer layer as taken from the RDF). The velocity exchange in this geometry occurs between CNT atoms and polymer carbon atoms in the slab with maximum separation in the z direction from the CNT. Eqn (3) is adopted to calculate the interfacial thermal conductivity λ_i. Note that the heat flux in eqn (3) is similarly defined as the one in eqn (1). Also note that the interfacial thermal conductivity λ_i is calculated perpendicular to the longitudinal CNT axis.

3. Computational conditions

In analogy to former simulation studies[26,54] we have performed atomistic MD simulations on a free PA matrix defined by 96 tetramers. This size restriction had to be accepted as response to the large computer time demand to equilibrate longer polymer chains. Although the chosen PA units are rather short, they show a static and dynamic behavior characteristic for longer polymer chains.[55] The flexible united-atom force field, f1-UA, described in ref. 56 has been employed for the polymer matrix. In this degree of sophistication the CH_2 and CH_3 groups are

considered as uncharged united atoms. In contrast to these uncharged fragments, the amide hydrogens, carbons and nitrogens as well as the oxygen atoms carry nonzero charges in the adopted f1-UA force field. Lussetti *et al.*[56] showed that the best agreement between calculated and experimental λ values of PA chains is observed when neglecting the high-energy modes associated to hydrogen stretching. The flexible f1-UA force field has also been used for the amide linkers employed for the nanotube functionalization. To model the grafted PE chains we have adopted the united atoms force field originally introduced by Paul *et al.*[57] Also this force field couples the hydrogen and carbon atoms of the CH_2 and CH_3 moieties to a single united atom fragment. The conformational degrees of freedom of a fully atomistic description, however, are taken into account in this approach. The PE chains grafted to CNT contain either 10, 20 or 40 united atom methylene groups, corresponding to $L = 5, 10, 20$ monomers. Methyl groups have been used at the chain ends. The considered dimensions allowed us to study the influence of the grafted chain length on quantities of interest. For the grafted PA chains only 10 monomers have been investigated. The MD simulations have been performed for different grafting densities. The force field parameters of Li and Chou[58] have been chosen for the CNT unit. The same setup had been adopted in our previous MD simulations of CNT samples.[14,26,27,33,52] The Lorentz–Berthelot mixing rule has been used to describe the interaction between the polymer matrix and the nanotube.[59]

To model nanocomposites with a functionalized CNT embedded in the PA matrix, we have selected an armchair nanotube of the (10,10) type with a length of 10 nm. The grafted chains have been connected with this CNT. All nanocomposites have been studied in a simulation cell with periodic boundary conditions both in the longitudinal and transversal CNT directions. Two snapshots of the simulation box containing either an ungrafted or a grafted CNT as well as the PA matrix surrounding the CNT are displayed in Fig. 1. The density of grafted chains (gd) is defined by the number of chains grafted to CNT atoms by chemical bonds. In addition to the ungrafted system gd = 0, we have chosen grafting densities of 0.5, 1.0, 3.0, and 5.0%. The functionalization is performed by randomly selecting grafting sites, *i.e.*, carbon atoms, that are—by new bonds—tethered with polymer atoms. Grafted PA and PE chains have been attached to CNT atoms by amide linkers, a method frequently used in experiments.[60] By the creation of the amide bonds on the CNT surface, we have prepared the chemical prerequisite for "covalent" functionalization with different chemical groups.[61] In this step we have to modify the force field parameters of the CNT atoms connected to the amide linker from an "sp^2" like characteristics to an "sp^3" one. Due to the bonding interactions between grafted chain atoms and CNT carbons, the functionalized tube centers are slightly deformed into the radial direction.[27] Thus these tube atoms do not participate in a perfect cylindrical CNT shape. Additionally, the bond lengths and bond angles at these perturbed CNT centers have been reparametrized. For carbon atoms bonded to these sp^3 CNT atoms no torsional potential has been considered. The new "covalent" bonds between the sp^3 like tube atoms and the amide linker coupling site have a length of 0.153 nm.[62] According to
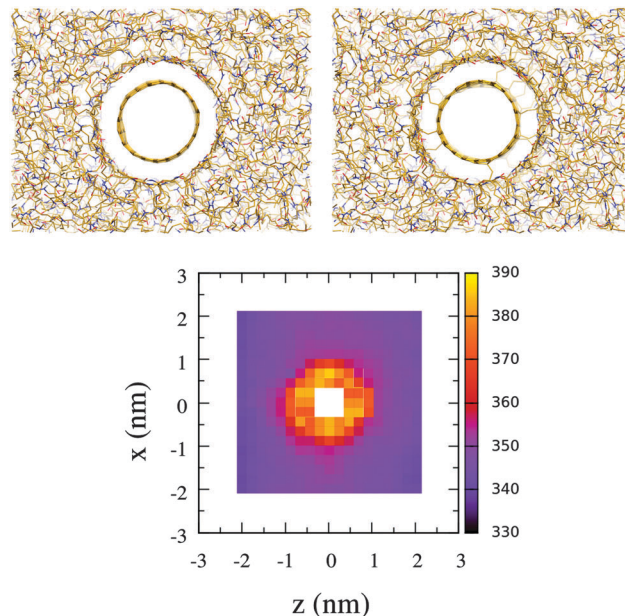

Fig. 1 Plot of the cross sectional area of a PA matrix in contact with an ungrafted CNT (upper left) as well as with a grafted CNT (upper right). The CNT is localized in the center of the simulation box. The bottom diagram shows the temperature profile of a nanocomposite containing a PE grafted CNT with a grafting density of 0.5%. The mean temperature amounts to 350 K. Note that the blank central area symbolizes the hollow inner CNT region.

density functional (DFT) calculations the C–C bond length adjacent to the bonded sp^3 like carbon atoms increases from 0.142 to 0.151 nm. For the bond angles under participation of the grafting CNT centers a decrease from 120° to 113.6° has been observed.[63,64]

To generate the starting configuration we filled the large initial simulation boxes by the predefined number of the PA chains and the PA or PE functionalized CNT. The density of these samples has been very low. After a short initial run of 3 ns under *NVT* conditions the systems have been simulated for 20 ns under isothermal–isobaric (*NPT*) conditions to reach equilibrium. Thereby the temperature has been fixed to 350 K; this has been done using a Berendsen thermostat. Possible pressure variations have been suppressed using a Berendsen barostat to conserve the chosen 101.3 kPa pressure. The calculated 350 K densities of roughly 1.081 g cm^{-3} were in good agreement with measured data (1.07 g cm^{-3} < ρ < 1.14 g cm^{-3}).[26] All MD runs were performed using the YASP package.[53] Nonbonded interactions between atoms coupled by torsional terms were fully considered. All nonbonded interactions were truncated at 1 nm with a reaction field correction for the Coulombic interactions. To simulate the screening of the electric charges in the matrix, we have chosen a relative permeability of 5.[65,66] We have used an atomic Verlet neighbor list with a cutoff radius of 1.1 nm updated at an interval of 15 time steps. Simulated configurations were sampled every 10 000 time steps (10 ps). For the leap-frog integration scheme a time step of 1.0 fs has been chosen. Having observed an equilibrated configuration for each system, the NEMD simulations were performed for a period of 4 ns using the

described setup. In the calculation of the interfacial thermal conductivity, the simulation box were divided into 20 slabs in the direction of the heat flow and into 12 slabs in the direction perpendicular to the heat flux which refers to the CNT axis. The atom velocities have been exchanged in a 0.3 ps interval. We have checked that the thermal conductivity converged within this exchange period. A typical temperature profile, in which the nanotube acts as hot region in contact with PA chains, can also be seen in Fig. 1. A complete description of the RNEMD method has been given in one of our recent publications.[52] The current computational parameters agree with the ones of this precursor study.[26]

4. Results and discussion

4.1 Polymer density in the vicinity of the nanotube

Recent computational studies verified the formation of a (highly) ordered polymer structure in the neighborhood of nanoparticles.[14,54,55,67] Fig. 2 displays the normalized density ρ/ρ^0 of the studied systems with ρ^0 denoting the bulk density of bare PA. The normalized density allows a fast comparison with the bare polymer. We have plotted ρ/ρ^0 for all polyamide-6,6 chains as well as for the two types of grafted PA and PE chains. The normalized density has been calculated by collecting the atoms of the PA matrix and the grafted chains within radial bins of 0.01 nm thickness around the nanotube. In all calculations we have taken the position of the nanotube cylinder surface to define the nanotube radius.

Fig. 2(a) presents the normalized density profile of all polymer chains, *i.e.* the free and grafted ones, as a function of the PE grafting density, gd. All PE chains grafted on the nanotube have the same length of 10 monomers. The density profiles of the grafted PE chains in the samples of Fig. 2(a) are shown in Fig. 2(b). While the normalized density ρ/ρ^0 of all polymer chains in Fig. 2(a) has been portrayed as a function of grafting density, Fig. 2(c) provides the same quantity for a common grafting density of 5% as a function of the length of the grafted chains. The grafted chains pendant of Fig. 2(c) is given in Fig. 2(d).

In the two diagrams presenting the overall polymer density, *i.e.* 2(a) and 2(c), we see oscillating density profiles indicating the ordering influence of the nanotube. This pattern has to be traced back to a forbidden volume effect. It is observed irrespective of the sign of the nanoparticle–polymer interaction.[67,68] In the two diagrams just mentioned, (a) and (c), we can identify three layers which are prevailingly caused by free PA chains. Fig. 2(b) and (d) show that this pattern does not occur for the grafted chains. The first density maximum in the full density profiles appears at a nanoparticle separation of 0.375 nm. In the ungrafted sample, the PA density at this position exceeds the PA bulk value by a factor of 2.5. For the highest grafting density this effect is reduced to a factor of roughly 1.2. The correlation of ρ/ρ^0 as a function of the grafting density with a fixed length (Fig. 2(a)) and the ρ/ρ^0 profile derived as a function of the length of the grafted chains for a common grafting density (Fig. 2(c)) shows large similarities of both profiles. For the ungrafted nanocomposites we find the second (third) density maximum roughly 0.8 (1.15) nm away
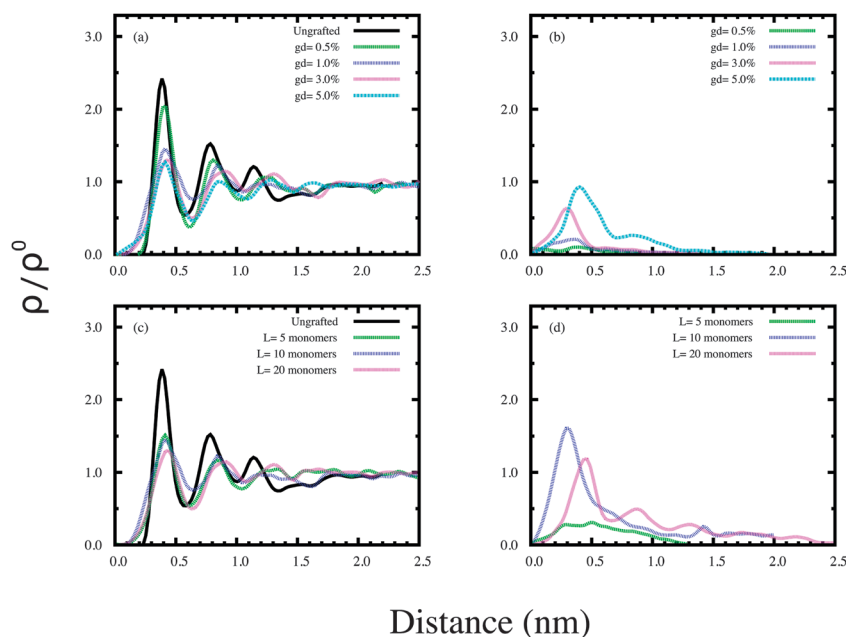
Fig. 2 Normalized density profile of all (grafted and free) polymer chains (diagrams a and c) and of the grafted chain atoms (diagrams b and d) as a function of the distance from the CNT surface. Panel (a) shows the normalized number density profiles of all polymer chains as a function of the grafting density gd starting from the ungrafted CNT. In (b) the density profiles of the grafted chains in the samples collected in (a) are displayed. Panel (c) represents again the overall normalized density profile for a PE grafting density of 5% as a function of the length of the free PA chains L. In analogy to (b), plot (d) provides again the density profile of the grafted PE chains for the samples of diagram (c). The average temperature of the simulations amounts to 350 K.

from the CNT surface. With increasing grafting density as well as with increasing length of the grafted chains these ρ/ρ^0 maxima are shifted to enlarged separations from the CNT unit. The splitting between the ρ/ρ^0 maxima in the ungrafted and grafted samples increases from the first to the third maximum. Again we notice that an increasing grafting density and length of the grafted chains have a similar influence on the profile and maxima of the ρ/ρ^0 curves.

The normalized density profiles in Fig. 2 lead to an inter-phase width not exceeding 1.5 to 1.6 nm. For larger separations from the CNT, ρ/ρ^0 is identical to the PA bulk density. The present findings agree with the results of older simulations.[55,67] Very recently, however, it has been shown that the interphase dimension estimated computationally does not only depend on the quantity considered but also for a given quantity, *e.g.* the heat of adsorption, on the chemistry of the probe particle.[68]

We want to summarize the trends that can be extracted from Fig. 2. The height of the density peaks is reduced with increasing CNT grafting. The density oscillations are largest for the ungrafted sample. Similar trends have been reported in other materials.[55,67] When looking for a simple interpretation of our simulation data we can classify the grafted chains as medium isolating the CNT unit from the surrounding polymer matrix. We find that the grafted chains are closer to the CNT surface than the ungrafted ones. This can be deduced when comparing the normalized density profiles of grafted chains in Fig. 2(b) and (d) with the ungrafted samples shown in Fig. 2(a) and (c). Our diagrams also indicate that the positions of the ρ/ρ^0 maxima for the grafted chains (see again Fig. 2(b) and (d)) cannot be related simply to the grafted chain length or grafting density. This has its origin in modifications in the orientation of the grafted chains as a function of these parameters. A "collapse" or adsorption of the grafted chains on the CNT surface implies a shift of their density profile towards the CNT surface.

4.2   Chain conformation and orientation

To study the influence of grafting on the conformation of the free PA chains, we analyze their mean-squared radius of gyration $\langle R_g^2 \rangle$, and—to smaller extend—their mean-squared end-to-end distance, $\langle R_{ee}^2 \rangle$, around a grafted CNT as a function of the grafting density and the grafted chain length. Fig. 3 provides $\langle R_g^2 \rangle$ profiles again sampled with the help of the adopted shell construction with a thickness of 0.01 nm. The assignment to the different shells is based on the center-of-mass of the chains. Recently Ndoro *et al.*[67] reported that the polymer $\langle R_g^2 \rangle$ is enlarged near (separation <0.5 nm) a nanoparticle. A polymer elongation in the host matrix layer around the nanoparticle (adsorption layer) of roughly 25% has been estimated some time ago.[69] Karatrantos *et al.*[70] discussed modifications in the local structure of the polymer matrix near a single-walled CNT surface which takes place under conservation of $\langle R_g^2 \rangle$. The results in Fig. 3 emphasize an elongation of the PA chains in the vicinity of the nanoparticle relative to the bulk behavior.

In the two diagrams, the PA bulk value $\langle R_g^2 \rangle \approx 0.66 \pm 0.02$ is symbolized by a broken horizontal line. For the grafting densities (bottom diagram) and grafted polymer lengths (top diagram)
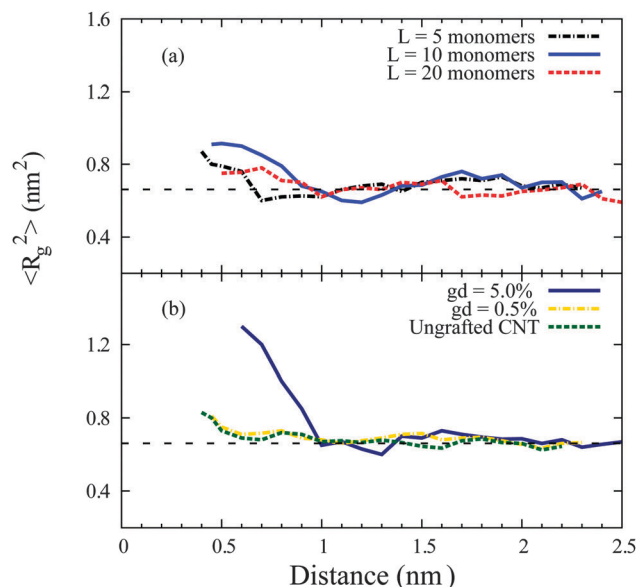

Fig. 3 Squared radius of gyration, $\langle R_g^2 \rangle$, of the free PA chains in the vicinity of an ungrafted or grafted CNT. The influence of different lengths of grafted PE chains (with a fixed gd = 5.0%) on the squared radius of gyration is depicted in panel (a). In (b) grafting densities of 0.5 and 5.0% have been considered. Here the length of the grafted PE chains amounts to 10 monomers. The dashed horizontal line in the two plots refers to the bulk value $\langle R_g^2 \rangle$ of bare PA. The radii of gyration have been calculated as a function of the center-of-mass separation of the PA chains from the nanotube.

chosen in Fig. 3, we see that the grafting density has a larger influence on $\langle R_g^2 \rangle$ than the length of the grafted chains. A strong variation of $\langle R_g^2 \rangle$ as a function of the length L of the grafted chains ($L = 5, 10, 20$) is not observed. The CNT-near elongation of PA chains in the polymer network with $L = 10$ exceeds slightly the $\langle R_g^2 \rangle$ increase in the other two samples ($L = 5, 20$). This deviation from simple expectations indicates that the grafted PE chains with 10 monomers have the strongest influence on the stretching of the free PA chains. From Fig. 3 we extract a bulk-like behavior of $\langle R_g^2 \rangle$ for separations from the nanoparticle around 1 nm, *i.e.* at a distance that is smaller than the interphase estimate on the basis of normalized densities. Such differences in the estimation of interphase extensions by molecular simulations has been emphasized already above.[68] In addition to $\langle R_g^2 \rangle$ we have also calculated its parallel and perpendicular components with respect to the CNT axis as a function of the separation between free PA chains and the CNT (not shown). As expected, near the nanotube the parallel $\langle R_g^2 \rangle$ component increases at the cost of the perpendicular element.

To provide some quantitative information on mean chain conformations, we have prepared Table 1 which contains $\langle R_g^2 \rangle$ as well as the mean-squared end-to-end distance $\langle R_{ee}^2 \rangle$ sampled over all free PA chains. The results, which are either derived as a function of the PA grafting density or as a function of the length of the grafted PE chains at a constant PE grafting density of 5%, have been related to the bulk parameters of pure PA. The first series of CNT modifications (*i.e.* grafting density, top part of the table) follows simple expectations. The $\langle R_g^2 \rangle$ and $\langle R_{ee}^2 \rangle$ elements

Table 1 Mean-squared radius of gyration $\langle R_g^2 \rangle$ and mean-squared end-to-end vector $\langle R_{ee}^2 \rangle$ of the free PA chains in nanocomposites with different grafting densities of PA chains with constant length or different lengths of the grafted PE with constant grafting density. The first numbers in the $\langle R_g^2 \rangle$ and $\langle R_{ee}^2 \rangle$ columns are the statistical mean values, the second ones the standard deviations

Systems	R_g^2 (nm^2)	R_{ee}^2 (nm^2)
Pure PA matrix	0.66 ± 0.02	2.85 ± 0.18
[Ungrafted CNT]–[PA] matrix	0.89 ± 0.03	3.02 ± 0.14
[0.5% PA grafted CNT]–[PA] matrix	0.91 ± 0.06	3.57 ± 0.20
[1% PA grafted CNT]–[PA] matrix	0.93 ± 0.04	4.04 ± 0.10
[3% PA grafted CNT]–[PA] matrix	1.00 ± 0.03	4.75 ± 0.29
[5% PA grafted CNT]–[PA] matrix	1.21 ± 0.08	5.42 ± 0.27
[5% PE grafted CNT with 5 monomers]–[PA] matrix	0.91 ± 0.03	3.61 ± 0.11
[5% PE grafted CNT with 10 monomers]–[PA] matrix	1.01 ± 0.02	3.76 ± 0.17
[5% PE grafted CNT with 20 monomers]–[PA] matrix	0.81 ± 0.05	3.16 ± 0.11

increase slightly with increasing grafting density. The length of the grafted chains is constant. Note that the calculated differences are within the error bars. All composite values of $\langle R_g^2 \rangle$ are much larger than the radius of gyration in the bulk. Quite generally, the same behavior is observed for $\langle R_{ee}^2 \rangle$. Such a regular variation as encountered for the grafting density variation is not realized as a function of the length of the grafted PE chains for a constant grafting density of 5%. The two squared length parameters are largest in the sample of grafted PE with $L = 10$ monomers. The stretching of the free PA chains is here more pronounced than in the case of the larger free chains containing 20 monomers. This could be extracted from Fig. 3 providing local values of $\langle R_g^2 \rangle$. The enlarged $\langle R_g^2 \rangle$ and $\langle R_{ee}^2 \rangle$ elements for the $L = 10$ chain in the table have to be traced back to the CNT-near elongation on the polymer chains. Finally please note the sizeable length reduction for the free PA chains with grafted PE of $L = 20$.

The orientation of the free PA bonds and their alignment around the CNT can be expressed by the angle $\theta(r)$ defined between the CNT axis and four consecutive PA bonds. The index (r) in $\theta(r)$ characterizes the distance dependence between the nanotube and the free PA chain under consideration. The second Legendre polynomial of $\cos\theta$, i.e., $(P_2(r) = (\frac{1}{2})(\langle 3\cos^2\theta_{i,j}\rangle - 1))$, describes the orientation of the PA chain relative to the CNT.[71] $P_2(r)$ spans a range between -0.5 and $+1.0$. The first boundary characterizes polymer segments perpendicular to the CNT axis. The second one refers to a parallel orientation. $P_2(r) = 0$ denotes complete random orientation of the "free" PA chains. Fig. 4 shows the distance dependence of $P_2(r)$ of the free PA chains sampled in the same bins as used for the calculation of the normalized mass density or the radius of gyration. Under the influence of the wrapping process around the tube, the polymer segments very close to the CNT orient preferentially perpendicular to the tube axis. The free PA chains at larger distances from the nanotube prefer to orient parallel to the tube axis. The same arrangement had been observed in previous simulation studies.[14,67,72] With increasing grafting density the maximum of the $P_2(r) > 0$ region is shifted to larger separations from the CNT surface. This reflects the increasing forbidden volume in the CNT vicinity with enlarged gd values. Beyond this "parallel domain" our atomistic simulations predict a series of minor minima and maxima in the $P_2(r)$ profile before approaching a random orientation at larger separations, i.e. $P_2(r) \approx 0$.
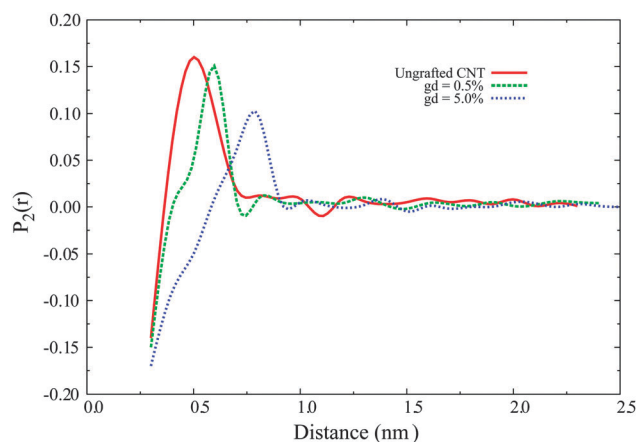
Fig. 4 Second Legendre polynomial $P_2(r)$ between four consecutive PA bonds and the CNT axis vector as a function of the separation r from the tube surface for the free PA chains. Both an ungrafted CNT and PA grafted tubes with grafting densities of 0.5 and 5.0% have been considered. The data have been sampled in the bins explained in the text. A positive (negative) order parameter $P_2(r)$ indicates a bond orientation parallel (perpendicular) to the CNT surface. $P_2(r) \approx 0$ characterizes random orientation.

The influence of the grafted chains on the orientational preferences of the free PA chains in the vicinity of the CNT is reduced with increasing grafting density.

From Fig. 4 we can extract the following general trends. For the shortest separation from the CNT surface ($P_2(r) < 0$) the ordering of the free chains is larger in the system with the highest grafting density (largest curve area in the $P_2(r) < 0$ domain). In the intermediate domain ($P_2(r) > 0$) the second Legendre polynomial has the highest maximum in the ungrafted CNT sample (highest peak and largest area).

The distribution function of the orientational angle θ (wrapping angle) of the grafted PE chains as a function of their lengths is given in Fig. 5. To measure θ we have adopted the same bin structure as explained above for the free PA chains. It can be seen in the figure that the wrapping angle for the all grafted chains lengths does not have a preferential orientation perpendicular to the tube axis. It seems that this is hindered by the interaction between atoms of the grafted chains and the CNT atoms. As response, the grafted chains show the tendency to attach the CNT surface. The chain orientation perpendicular to the CNT axis is smallest for the grafted chains with the
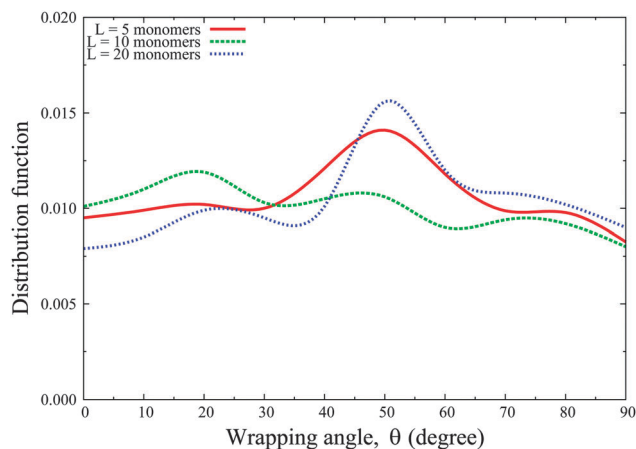
Fig. 5 Distribution functions of the orientational angle between four consecutive PA bounds and the nanotube axis. The CNT is grafted by PE chains with different lengths. The grafting density amounts to 5%. The curves have been smoothed for convenience of the eye.
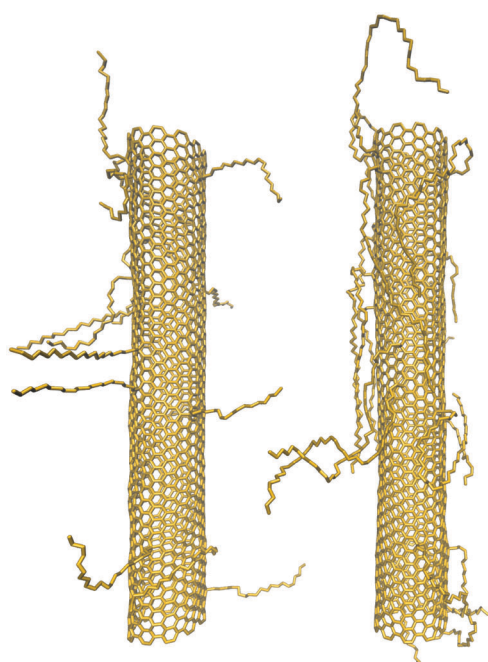

Fig. 6 Arrangement of the grafted PE chains in nanocomposites with a length of 10 (left diagram) and 20 monomers (right diagram).

Fig. 7 Calculated interfacial thermal conductivity λ_i in the studied PA–CNT composites with grafted PE as derived by RNEMD simulations at T = 350 K. λ_i has been evaluated perpendicular to the longitudinal CNT axis. It has been measured between the CNT and the first PA layer. Cylindrical interfaces have been employed. The λ values confined to the dotted curve correspond to the ungrafted sample. In the upper three curves both the influences of the grafting density and PA chains lengths have been considered. The vertical lines are the computational error bars.

grafted chains is a key quantity to tailor the structural properties of polymers in the interphase region of CNT-containing nanocomposites.

4.3 Interfacial thermal conductivity in nanocomposites

In the two last subsections we have discussed the structural properties of the considered CNT containing PA composites. These data have been derived by equilibrium MD calculations. Now we will show that the polymer structure in the interphase region has a decisive influence on the interfacial thermal conductivity. Fig. 7 provides λ_i of the composite with an ungrafted CNT and the composites with a grafted nanotube. For the latter nanocomposites we have evaluated λ_i both as a function of this grafting density and the monomer number L. The λ_i value of the ungrafted composite does not exceed 0.003 W mK^{-1}. For the composites with a PE grafted CNT, λ_i numbers between 0.02 and 0.07 W mK^{-1} are derived by the present RNEMD simulations. These λ_i parameters exceed the thermal conductivity of the composite with an ungrafted nanotube by one order of magnitude. Due to the present definition of λ_i a direct comparison with the thermal conductivity of bare PA samples but also with composites is not possible. Recently Ding *et al.*[73] published an experimental study of nanocomposites in which graphene is covalently grafted by polyamide-6 (PA6). In analogy to the present simulation work they found that the thermal conductivity is reduced (from 0.293 to 0.265 W mK^{-1}) when the length of the PA6 chains is enlarged. Our discussion of structural properties of grafted CNTs in a polymer matrix provides an explanation of these experimental data. We simply assume that the penetration of the grafted chains into the polymer matrix is again increasingly hindered with increasing chain length.

Let us have a look onto the phonon density of states profiles in Fig. 8 confined to the CNT and grafted chain atoms forming

largest number of monomers (L = 20). The largest perpendicular orientation of the grafted chains is realized in the sample with 10 monomers. This differs from the simple expectation to have the maximum penetration and mixing of the grafted chains with the polymer matrix in the L = 20 system.

Representative orientations of the grafted chains in samples with 10 (left hand side) or 20 (right hand side) monomers can be seen in Fig. 6. The chain wrapping in the sample with 20 monomers exceeds the one in the 10 monomer example. Thus, entanglements between the grafted chains and the surrounding polyamide chains in the L = 20 case are smaller than expected. Thus we can deduce that the length of the
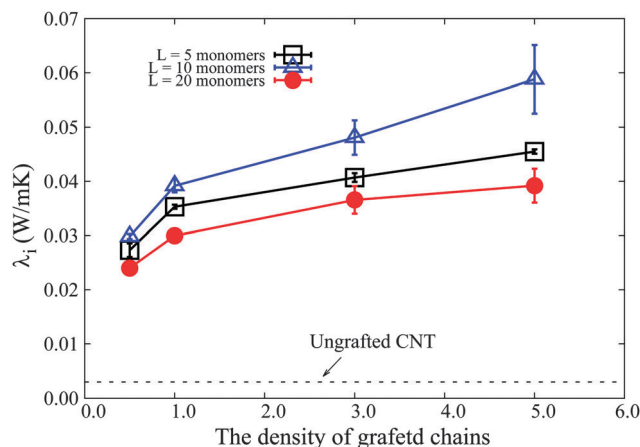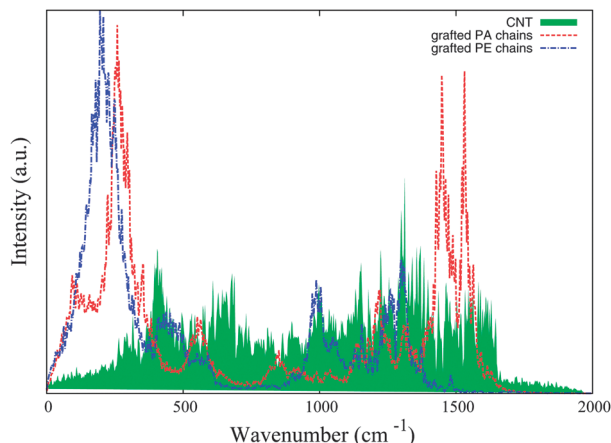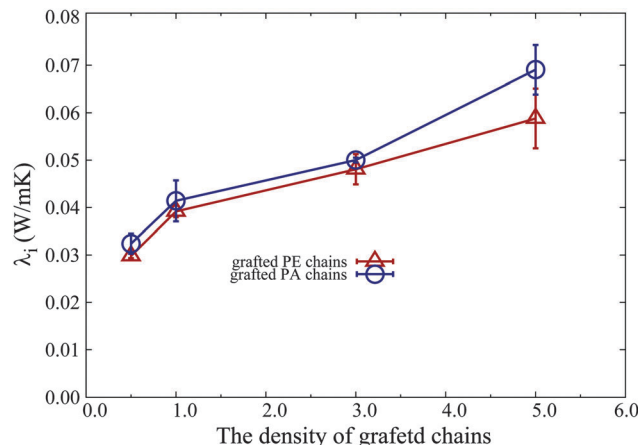
Fig. 8 Phonon density of states confined to the sp^3 like CNT atoms and the CNT bonded atoms of the grafted PE and PA chains. The grafting density amounts to 5% and the length of the PE grafted chains to 10 monomers as well as PA grafted have roughly similar length. The phonon DOS have been calculated *via* the velocity autocorrelation function at T = 350 K.

Fig. 9 Interfacial thermal conductivity λ_i observed in a PE and PA grafted CNT as a function of the grafting density. The length of the grafted PE and PA chains containing 10 monomers is roughly similar. The RNEMD simulations have been performed at 350 K. The vertical lines represent the error bars of the simulations.

the chemical bonds between both components in the case of grafting. The phonon DOS profiles of the relevant atoms are obtained from equilibrium MD simulations. The average velocity autocorrelation function has been computed from five trajectories sampled over 8 ps and a mutual time separation of 200 ps. Then the average velocity autocorrelation function was transformed by Fourier transform yielding the power spectra. A time interval of 1 fs between two adjacent data points has been chosen. A more detailed description of the employed formalism can be found in one of the our recent articles.[14] When computing the phonon DOS profiles of the atoms forming the PA–CNT bonds, we see that grafting provides new low-energy modes relevant for a vibrational support of thermal conductivity. It can be assumed that these modes allow an energy transport from the CNT to the grafted chains. Irrespective of the efficiency of this vibrational coupling, the grafted chains reduce the number of weak van der Waals contacts with their λ_i attenuating Kapitza resistances.

With the knowledge provided by the phonon DOS profiles in Fig. 8 we can go back to the λ_i plot of Fig. 7. The λ_i enhancement from the ungrafted sample to the grafted ones and the increasing thermal conductivity with an increasing number of grafted chains is in line expectations that follow from the present argumentation. The λ_i maximum for the grafted chains of intermediate length (L = 10) has its origin in the higher CNT attachment of the L = 20 chains leading to a less efficient collision coupling between the polymer matrix and the grafted chains than accessible in the L = 10 example.

The interfacial thermal conductivity for PE and PA grafting is compared in Fig. 9 as a function of the grafting density. The increase of λ_i with increasing grafting density follows a trend already discussed; check again Fig. 7. In Fig. 9 we see that the interfacial thermal conductivity in PA grafted samples is slightly larger than the one in the PE grafted pendant. The splitting is more pronounced for samples with higher grafting densities.

The present results are in line with expectations following from the presence (PA) or absence (PE) of hydrogen bridges (HBs) provided by the grafted chains. The experimental work of Kim *et al.*[74] indicates an enhancement of the thermal conductivity under the influence of HBs. In the samples studied in the present work, the average number of HBs per chain is less than one (not shown here). Therefore their influence on the interfacial thermal conductivity cannot be strong. Now let us reconsider Fig. 8. We can deduce that both types of grafted chains provide vibrational modes with small wave numbers leading to a phonon support of the interfacial thermal conductivity. But on the basis of the present qualitative discussion of the phonon DOS profiles alone, it is impossible to explain the slightly higher thermal conductivity values in the case of PA grafting. Thus it seems to be not unreasonable to explain the slightly larger λ_i in the PA grafted samples by hydrogen bonding.

5. Summary and conclusion

We have performed reverse nonequilibrium MD simulations of carbon nanotube–PA oligomer nanocomposites to explain the influence of chemical CNT functionalization on the interfacial thermal conductivity. Particular attention has been focused on the influence of the grafting density and grafting chain length as well as of the grafted chain chemistry on the interfacial thermal conductivity. An interpretation of these RNEMD results has been possible when adopting structural data of the free and grafted polymer chains in the vicinity of the CNT. Both the ungrafted CNT and the grafted nanotubes support an ordering of the polymer matrix allowing a more efficient heat transport. The effect of the grafting on the structure of the polyamide matrix has been quantified by several quantities, *i.e.* density profiles, the polymer radius-of-gyration and end-to-end distance as a function of the separation from the CNT surface as well as the gyration tensor. For a better understanding, the chain orientations of the free and grafted chains have been investigated

separately. The ordered polymer matrix structure in the interphase could be quantified by enlarged values of the radius-of-gyration or the end-to-end vector. As could be assumed *a priori* the influence of grafting on matrix properties is enhanced with increasing grafting density. Such a clear trend is not observed when considering the influence of the length, *i.e.*, number of monomers, of the grafted chains on the PA matrix. Here we have detected that the grafted chains with an intermediate number of monomers, $L = 10$, penetrate and couple stronger to the surrounding matrix than the shortest grafted chains, $L = 5$. For the $L = 5$ chains this is expected while it is not for the $L = 20$ system. However, the prominent behavior of the $L = 10$ grafting could be explained by the L dependent association of the grafted chains to the CNT. The surface association in the $L = 20$ sample exceeds the $L = 10$ case. In contrast to the remarkable influence of the grafting density and length of the grafted chains on the interfacial thermal conductivity, the chemical differences (*e.g.* capability to form HBs) between PA and PE grafting of roughly the same grafting length seems to be not large enough to cause sizable differences in the calculated λ_i values. Simulations with higher concentration of grafted PA and PE chains would be useful to clarify the influence of hydrogen bridges on the thermal conductivity in the chosen CNT nanocomposites more precisely.

An analysis of the vibrational density of states has shown that the grafted chains provide new vibrational modes of low wave numbers which support the energy transport in polymers. At the same time these "covalent" chemical bonds reduce the number of weak van der Waals contacts per unit volume with their λ reducing Kapitza resistances. The λ_i enhancement due to ungrafted and—in particular—due to grafted CNTs has been rationalized in detail. The present discussion of factors to enhance the heat transfer in (CNT enriched) polymer composites might be used as a guideline to tailor systems with high thermal conductivities.

Acknowledgements

Note and references

1 W. Guo, C. Liu, X. Sun, Z. Yang, H. G. Kiab and H. Peng, *J. Mater. Chem.*, 2012, **22**, 903–908.
2 Z. Spitalsky, D. Tasis, K. Papagelis and C. Galiotis, *Prog. Polym. Sci.*, 2010, **35**, 357–401.
3 F. H. Gojny, M. H. G. Wichmann, B. Fiedler and K. Schulte, *Compos. Sci. Technol.*, 2005, **65**, 2300–2313.
4 X. Xu, M. M. Thwe, C. Shearwood and K. Liao, *Appl. Phys. Lett.*, 2002, **81**, 2833–2835.
5 J. F. Vega, J. Martínez-Salazar, M. Trujillo, M. L. Arnal, A. J. Müller, S. Bredeau and Ph. Dubois, *Macromolecules*, 2009, **42**, 4719–4727.
6 H. Peng and X. Sun, *Chem. Phys. Lett.*, 2009, **471**, 103–105.
7 H. Ogihara, H. Kibayashi and T. Saji, *ACS Appl. Mater. Interfaces*, 2012, **4**, 4891–4897.
8 S. Li, Y. Qin, J. Shi, Z. Guo, Y. Li and D. Zhu, *Chem. Mater.*, 2005, **17**, 130–135.
9 S. U. S. Choi, Z. G. Zhang, W. Yu, F. E. Lockwood and E. A. Grulke, *Appl. Phys. Lett.*, 2001, **79**, 2252–2254.
10 S. Huxtable, D. G. Cahill, S. Shenogin, L. Xu, R. Ozisik, P. Barone, M. Usrey, M. S. Strano, G. Siddons, M. Shim and P. Keblinski, *Nat. Mater.*, 2003, **2**, 731–734.
11 F. Wu, X. He, Y. Zeng and H. M. Cheng, *Appl. Phys. A: Mater. Sci. Process.*, 2006, **85**, 25–28.
12 Y. A. Kim, S. Kamio, T. Tajiri, T. Hayashi, S. Song, M. Endo, M. Terrones and M. S. Dresselhaus, *Appl. Phys. Lett.*, 2007, **90**, 093125.
13 M. J. Biercuk, M. C. Llaguno, M. Radosavljevic, J. K. Hyun, A. T. Johnson and J. E. Fischer, *Appl. Phys. Lett.*, 2002, **80**, 2767–2769.
14 M. Alaghemandi, J. Schulte, F. Leroy, F. Müller-Plathe and M. C. Böhm, *J. Comput. Chem.*, 2011, **32**, 121–133.
15 A. E. Aliev, M. H. Lima, E. M. Silverman and R. H. Baughman, *Nanotechnology*, 2010, **21**, 035709.
16 A. A. Balandin, S. Ghosh, W. Bao, I. Calizo, D. Teweldebrhan, F. Miao and C. N. Lau, *Nano Lett.*, 2008, **8**, 902–907.
17 J. H. Seol, I. Jo, A. L. Moore, L. Lindsay, Z. H. Aitken, M. T. Pettes, X. Li, Z. Yao, R. Huang, D. Broido, N. Mingo, R. S. Ruoff and L. Shi, *Science*, 2010, **328**, 213–216.
18 Z. Han and A. Fina, *Prog. Polym. Sci.*, 2011, **36**, 914–944.
19 E. A. Algaer, M. Alaghemandi, M. C. Böhm and F. Müller-Plathe, *J. Phys. Chem. B*, 2009, **113**, 14596–14603.
20 D. N. Simavilla, J. D. Schieber and D. C. Venerus, *J. Polym. Sci., Part B: Polym. Phys.*, 2012, **50**, 1638–1644.
21 S. Gupta, J. D. Schieber and D. C. Venerus, *J. Rheol.*, 2013, **57**, 427–739.
22 K. Kurabayashi, *Int. J. Thermophys.*, 2001, **22**, 277–288.
23 F. Müller-Plathe, *J. Chem. Phys.*, 1996, **106**, 6082–6085.
24 D. Donadio and G. Galli, *Phys. Rev. Lett.*, 2007, **99**, 255502.
25 A. K. Roy, B. L. Farmer, V. Varshney, S. Sihn, J. Lee and S. Gangoli, *ACS Appl. Mater. Interfaces*, 2012, **4**, 545–563.
26 M. Alaghemandi, F. Müller-Plathe and M. C. Böhm, *J. Chem. Phys.*, 2011, **135**, 184905.
27 M. R. Gharib-Zahedi, M. Tafazzoli, M. C. Böhm and M. Alaghemandi, *J. Chem. Phys.*, 2013, **139**, 184704.
28 Z. Shen, S. Bateman, D. Y. Wu, P. McMahon, M. Dell'Olio and J. Gotama, *Compos. Sci. Technol.*, 2009, **69**, 239–244.
29 M. B. Bryning, D. E. Milkie, M. F. Islam, J. M. Kikkawa and A. Yodh, *Appl. Phys. Lett.*, 2005, **87**, 161909.
30 F. Du, C. Guthy, T. Kashiwagi, J. E. Fischer and K. I. Winey, *J. Polym. Sci., Part B: Polym. Phys.*, 2006, **44**, 1513–1519.
31 A. P. Yu, P. Ramesh, X. B. Sun, E. Bekyarova, M. E. Itkis and R. C. Haddon, *Adv. Mater.*, 2008, **20**, 4740–4744.
32 H. M. Duong, D. V. Papavassiliou, K. J. Mullen and S. Maruyama, *Nanotechnology*, 2008, **19**, 065702.
33 M. Alaghemandi, F. Leroy, F. Müller-Plathe and M. C. Böhm, *Phys. Rev. B: Condens. Matter Mater. Phys.*, 2010, **81**, 125410.

34 S. Niyogi, M. A. Hamon, H. Hu, B. Zhao, P. Bhowmik, R. Sen, M. E. Itkis and R. C. Haddon, *Acc. Chem. Res.*, 2002, **135**, 1105–1113.

35 N. G. Sahooa, S. Ranab, J. W. Chob, L. Lia and S. H. Chan, *Prog. Polym. Sci.*, 2010, **35**, 837–867.

36 J. Gao, M. E. Itkis, A. Yu, E. Bekyarova, B. Zhao and R. C. Haddon, *J. Am. Chem. Soc.*, 2005, **127**, 3847–3854.

37 O. Morales-Teyssier, S. Sanchez-Valdes and L. F. Ramos-de Valle, *Macromol. Mater. Eng.*, 2006, **291**, 1547–1555.

38 M. Moniruzzaman and K. I. Winey, *Macromolecules*, 2006, **39**, 5194–5205.

39 C. Baudot and C. M. Tan, *Carbon*, 2011, **49**, 2362–2369.

40 J. Gyu Park, Q. Cheng, J. Lu, J. Bao, S. Li, Y. Tian, Z. Liang, C. Zhang and B. Wang, *Carbon*, 2012, **50**, 2083–2090.

41 J. Huang, M. Gao, T. Pan, Y. Zhang and Y. Lin, *Compos. Sci. Technol.*, 2014, **95**, 16–20.

42 W.-L. Song, W. Wang, L. Monica Veca, C. Y. Kong, M.-S. Cao, P. Wang, M. J. Meziani, H. Qian, G. E. LeCroy, L. Caoa and Y.-P. Sun, *J. Mater. Chem.*, 2012, **22**, 17133–17139.

43 R. Gulotty, M. Castellino, P. Jagdale, A. Tagliaferro and A. A. Balandin, *ACS Nano*, 2013, **7**, 5114–5121.

44 A. Bagchi and S. Nomura, *Compos. Sci. Technol.*, 2006, **66**, 1703–1712.

45 G. D. Seidel and D. C. Lagoudas, *J. Appl. Mech.*, 2008, **75**, 041025.

46 F. Gardea, M. Naraghi and D. Lagoudas, *ACS Appl. Mater. Interfaces*, 2014, **6**, 1061–1072.

47 T. C. Clancy and T. S. Gates, *Polymer*, 2006, **47**, 5990–5996.

48 K. S. Khare, F. Khabaz and R. Khare, *ACS Appl. Mater. Interfaces*, 2014, **6**, 6098–6110.

49 T. Luo and J. R. Lloyd, *Adv. Funct. Mater.*, 2012, **22**, 2495–2502.

50 M. Wang, D. Galpaya, Z. B. Lai, Y. Xu and C. Yan, *Int. J. Smart Nano Mater.*, 2014, **5**, 123–132.

51 M. Wang, N. Hu, L. Zhou and C. Yan, *Carbon*, 2015, **85**, 414–421.

52 M. Alaghemandi, E. Algaer, M. C. Böhm and F. Müller-Plathe, *Nanotechnology*, 2009, **20**, 115704.

53 F. Müller-Plathe, *Comput. Phys. Commun.*, 1993, **78**, 77–94.

54 M. Alaghemandi, M. R. Gharib-Zahedi, E. Spohr and M. C. B hm, *J. Phys. Chem. C*, 2012, **116**, 14115–14122.

55 H. Eslami, M. R. Rahimi and F. Müller-Plathe, *Macromolecules*, 2013, **46**, 8680–8692.

56 E. Lussetti, T. Terao and F. Müller-Plathe, *J. Phys. Chem. B*, 2007, **111**, 11516–11523.

57 W. Paul, D. Y. Yoon and G. D. Smith, *J. Chem. Phys.*, 1995, **103**, 1702–1709.

58 C. Li and T. W. Chou, *Int. J. Solids Struct.*, 2003, **40**, 2487–2499.

59 M. P. Allen and D. J. Tildesley, *Computer Simulation of Liquids*, Clarendon, Oxford, 1987.

60 E. Bekyarova, B. Zhao, R. Sen, M. E. Itkis and R. C. Haddon, *Prepr. Pap. - Am. Chem. Soc., Div. Fuel Chem.*, 2004, **49**, 936–937.

61 K. Balasubramanian and M. Burghard, *Small*, 2005, **1**, 180–192.

62 P. Lu, R. Zhou, W. Guo and X. C. Zeng, *J. Phys. Chem. C*, 2012, **116**, 13722–13730.

63 N. Al-Aqtash and I. Vasiliev, *J. Phys. Chem. C*, 2011, **115**, 18500–18510.

64 H. J. C. Berendsen, J. P. M. Postma, W. F. van Gunsteren, A. DiNola and J. R. Haak, *J. Chem. Phys.*, 1984, **81**, 3684–3690.

65 S. Goudeau, M. Charlot, C. Vergelati and F. Müller-Plathe, *Macromolecules*, 2004, **37**, 8072–8081.

66 S. Goudeau, M. Charlot and F. Müller-Plathe, *J. Phys. Chem. B*, 2004, **108**, 18779–18788.

67 T. V. M. Ndoro, E. Voyiatzis, A. Ghanbari, D. N. Theodorou, M. C. Böhm and F. Müller-Plathe, *Macromolecules*, 2011, **44**, 2316–2327.

68 E. Voyiatzis, M. Rahimi, F. Müller-Plathe and M. C. Böhm, *Macromolecules*, 2014, **47**, 7878–7889.

69 G. Milano, G. Santangelo, F. Ragone, L. Cavallo and A. Di Matteo, *J. Phys. Chem. C*, 2011, **115**, 15154–15163.

70 A. Karatrantos, R. J. Composto, K. I. Winey and N. Clarke, *Macromolecules*, 2011, **44**, 9830–9838.

71 D. Rigby and R.-J. Roe, *J. Chem. Phys.*, 1988, **89**, 5280–5290.

72 H. Eslami and M. Behrouz, *J. Phys. Chem. C*, 2014, **118**, 9841–9851.

73 P. Ding, S. Su, N. Song, S. Tang, Y. Liu and L. Shi, *RSC Adv.*, 2014, **4**, 18782–18791.

74 G.-H. Kim, D. Lee, A. Shanker, L. Shao, M. S. Kwon, D. Gidley, J. Kim and K. P. Pipe, *Nat. Mater.*, 2015, **14**, 295–300.